Fission and quasifission of composite systems with $Z = 108-120$: Transition from heavy-ion reactions involving S and Ca to Ti and Ni ions

E. M. Kozulin,[1] G. N. Knyazheva,[1] K. V. Novikov,[1] I. M. Itkis,[1] M. G. Itkis,[1] S. N. Dmitriev,[1] Yu. Ts. Oganessian,[1] A. A. Bogachev,[1] N. I. Kozulina,[1] I. Harca,[1,2] W. H. Trzaska,[3] and T. K. Ghosh[4]

[1]*Flerov Laboratory of Nuclear Reactions, Joint Institute for Nuclear Research, Dubna 141980, Russia*

[2]*Facultatea de Fizica, Universitatea din Bucuresti, Bucharest, Romania and H. Hulubei National Institute for R & D in Physics and Nuclear Engineering, Bucharest-Magurele, Romania*

[3]*Accelerator Laboratory, University of Jyväskylä, FI-40014, Finland*

[4]*Variable Energy Cyclotron Centre, Bidhan Nagar, Kolkata -700 064, India*

(Received 16 August 2016; published 10 November 2016)

Background: Suppression of compound nucleus formation in the reactions with heavy ions by a quasifission process in dependence on the reaction entrance channel.

Purpose: Investigation of fission and quasifission processes in the reactions ^{36}S ,^{48}Ca ,^{48}Ti, and ^{64}Ni + ^{238}U at energies around the Coulomb barrier.

Methods: Mass-energy distributions of fissionlike fragments formed in the reaction ^{48}Ti + ^{238}U at energies of 247, 258, and 271 MeV have been measured using the double-arm time-of-flight spectrometer CORSET at the U400 cyclotron of the Flerov Laboratory of Nuclear Reactions and compared with mass-energy distributions for the reactions ^{36}S ,^{48}Ca ,^{64}Ni + ^{238}U.

Results: The most probable fragment masses as well as total kinetic energies and their dispersions in dependence on the interaction energies have been investigated for asymmetric and symmetric fragments for the studied reactions. The fusion probabilities have been deduced from the analysis of mass-energy distributions.

Conclusion: The estimated fusion probability for the reactions S, Ca, Ti, and Ni ions with actinide nuclei shows that it depends exponentially on the mean fissility parameter of the system. For the reactions with actinide nuclei leading to the formation of superheavy elements the fusion probabilities are of several orders of magnitude higher than in the case of cold fusion reactions.

DOI: 10.1103/PhysRevC.94.054613

I. INTRODUCTION

The existence of an island of stability in the region of nuclei with $Z = 114$ and $N = 184$ predicted theoretically [1] caused the experimental investigation in the field of the superheavy element (SHE) synthesis. Nowadays more than 30 isotopes of superheavy elements with $Z = 108-118$ have been synthesized both in cold [2,3] and in hot fusion reactions [4–7]. In the Flerov Laboratory of Nuclear Reactions great success was achieved in the synthesis of superheavy elements in the hot fusion reactions of ^{48}Ca ions with actinide target nuclei. Unfortunately, nuclei with $Z > 118$ cannot be synthesized in ^{48}Ca-induced reactions since ^{249}Cf is the heaviest target material available for these purposes. One of the possible pathways to synthesize new isotopes of superheavy elements with $Z = 118-126$ is the reactions of actinide targets with Ti, Fe, and Ni ions.

The mechanism of fusion of massive nuclei is significantly different from the formation of a compound nucleus (CN) known in the case of light projectiles because of the substantial increase in the Coulomb repulsion between the interacting nuclei. It was shown experimentally [8–10] that at energies around the Coulomb barrier the complete fusion of two massive nuclei is suppressed by a competing binary process, the quasifission (QF) in which the composite system separates in two main fragments without forming a CN. QF happens to be the most important mechanism that prevents the formation of SHEs in the fusion of heavy nuclei.

The rise of the QF process as a hindering factor to complete fusion appears to be the main consequence of a complex collective motion in a stronger Coulomb field. For this reason, the cross section for producing a heavy evaporation residue (ER) $\sigma_{\rm ER}$ in a fusion reaction can be written as

$$\sigma_{\rm ER} = \sigma_{\rm capture} P_{\rm CN} W_{\rm survival}, \quad (1)$$

where $\sigma_{\rm capture}$ is the capture cross section, $P_{\rm CN}$ is the probability that after overcoming the Coulomb barrier the interacting nuclear system reaches a compact CN. $W_{\rm survival}$ is the probability that the CN survives against fission (CN fission). Experimentally, the capture cross section is defined as the sum of the QF, CN-fission, and ER cross sections,

$$\sigma_{\rm capture} = \sigma_{\rm QF} + \sigma_{\rm CN\text{-}fission} + \sigma_{\rm ER}. \quad (2)$$

The survival probability is a property of the CN and depends on the excitation energy of the CN and angular momentum. The main uncertainty in the determination of $\sigma_{\rm ER}$ gives the value of the fusion probability $P_{\rm CN}$. The experimental measurements of fusion probability show the general dependence of $P_{\rm CN}$ upon fissility. The predictions of theoretical models, for example [11–14], applied to describe the whole evolution of low-energy nucleus-nucleus collisions at strong channel coupling of deep-inelastic scattering, CN formation, and QF, strongly vary from each other. Especially for the reactions leading to the formation of SHEs, whereas all models describe rather well the ER cross sections, the values

of P_{CN} differ from each other by several orders of magnitude [15,16]. It is important to determine P_{CN} experimentally to improve the understanding of reaction mechanisms taking place in the reactions with heavy ions. Besides, the dependence of P_{CN} on interacting energy and the reaction entrance channel is not well established.

To define the experimental value of P_{CN} the information about the relative contributions of QF, CN fission, and ER components into the capture cross sections is needed. In the case of reactions leading to the formation of SHEs the ER cross section in negligibly small compared with CN-fission and QF processes. Since CN fission and QF are both binary decay channels characterized by large nucleon exchange and energy dissipation, it is difficult to perform the experimental separation between QF and CN fission. The experimental separation of CN fission and QF usually is based on the analysis of different experimental observables of fissionlike fragments, namely, angular distributions [16–19], width of mass distributions [13,20–22], mass and energy distributions [23–25], and mass and angular distributions [10,26–30]. In the reactions with heavy ions leading to the formation of SHEs, the method based on the analysis of mass and energy distributions [23–25] seems to be more reliable especially in the symmetric mass region. With this approach it is possible to estimate the upper limit of CN-fission yield into all capture events for the mass-symmetric fragments, whose angular distributions are symmetric with respect to 90° in the center-of-mass system and, consequently, cannot be used to distinguish between CN-fission and QF fragments.

The paper presents the results of the systematical study of fission and quasifission processes in hot fusion reactions with actinide targets. The properties of the mass and energy distributions of fissionlike fragments formed in the reactions ^{36}S ,^{48}Ca ,^{48}Ti, and ^{64}Ni + ^{238}U at energies around the Coulomb barrier have been analyzed. The reactions ^{36}S ,^{48}Ca, and ^{64}Ni + ^{238}U have been investigated earlier [23–25]. In the present paper, to define the systematic trend of CN fission and QF in hot fusion reactions with actinide targets, the mass and energy distributions of fissionlike fragments formed in the reaction ^{48}Ti + ^{238}U at energies around the Coulomb barrier have been measured.

II. EXPERIMENT

The experiment was carried out at the Flerov Laboratory of Nuclear Reactions using ^{48}Ti beams extracted from the U400 cyclotron at energies of 247, 258, and 271 MeV. The energy resolution was ∼1%. Beam intensities on target were 2 to 3 pnA. The target layer of ^{238}U 270-$\mu g/cm^2$ thick was coated with 10 $\mu g/cm^2$-thick carbon layers. The enrichment of the target layer was 99.99%. The details of the measurements of the mass and energy distributions for the reactions with ^{36}S ,^{48}Ca, and ^{64}Ni ions are given in Refs. [23,25].

For all studied reactions the binary reaction products were detected in coincidence by the double-arm time-of-flight spectrometer CORSET [31]. Each arm of the spectrometer consists of a compact start detector and a position-sensitive stop detector, based on microchannel plates. The arms of the spectrometer were positioned symmetrically at the angles of 67°, 64°, 64°, and 60° to the beam axis for the reactions ^{36}S ,^{48}Ca ,^{48}Ti, and ^{64}Ni + ^{238}U, respectively. With this choice of angles the fragments are detected at 90° in the center-of-mass frame in the case of symmetric splitting. The position resolution of the stop detectors equals 0.3°, and the time resolution is about 150 ps.

The mass and energy resolutions of the CORSET setup are taken as the FWHM of the mass and energy spectra, respectively, constructed for the elastic scattering. In the above conditions, the mass resolution of the spectrometer is ±2 u; the total kinetic energy (TKE) resolution is ±10 MeV. The adequate mass and energy resolutions of the spectrometer allow analyzing the binary fragments mass and energy distributions and their dispersions.

The data processing assumes standard two-body kinematics [31]. Primary masses, velocities, energies, and angles of reaction products in the center-of-mass system were calculated from the measured velocities and angles using the momentum and mass conservation laws with the assumption that the mass of the composite system is equal to $M_{target} + M_{projectile}$. Neutron evaporation before scission is not taken into account. This is justified by the fact that even at the highest reaction energies not more than four neutrons could be emitted. Hence, considering that the spectrometer resolution is 4 u, the neutron emission will not lead to visible effects on the mass-energy distributions. Corrections for the fragment energy losses through the target material, target backing, and the start detector foils were included in the data analysis.

The identification of the binary reaction channel with full momentum transfer and the removal of products of sequential and incomplete fission reactions, induced fission of target, and targetlike nuclei, or reactions on impurity atoms in the target were based on the analysis of the kinematic diagram (the velocity vectors of two detected reaction products) in the center-of-mass system [31]. For full momentum transfer events the distribution of the $V_\perp$ component of fragment velocity (projection of the fragment velocity vector onto the plane perpendicular to the beam axis) is expected to peak at zero, whereas the $V_{||}$ (projection of the fragment velocity vector onto the beam axis) should be equal to the calculated center-of-mass velocity for the collision $V_{c.m.}$. To remove background events $V_\perp$ and $V_{||}$ were gated with a $\pm 3\sigma$ contour that accepts 99% of full momentum transfer events.

III. RESULTS AND DISCUSSION

A. Mass-energy distributions of fissionlike fragments

Figure 1 displays the mass and energy distributions of binary fragments obtained in the reaction ^{48}Ti + ^{238}U. The reaction products having masses close to those of projectile and target are identified as quasielastic and deep-inelastic events in the TKE-mass (TKE,M) matrix. Reaction products lying between elastic peaks (outlined by the solid lines in the top panels) can be identified as totally relaxed events, i.e., as fission (or fissionlike) fragments. Henceforth we consider the properties of these events only. The mass-energy distributions for the reactions ^{36}S ,^{48}Ca, and ^{64}Ni + ^{238}U have already been reported in Refs. [23,25].

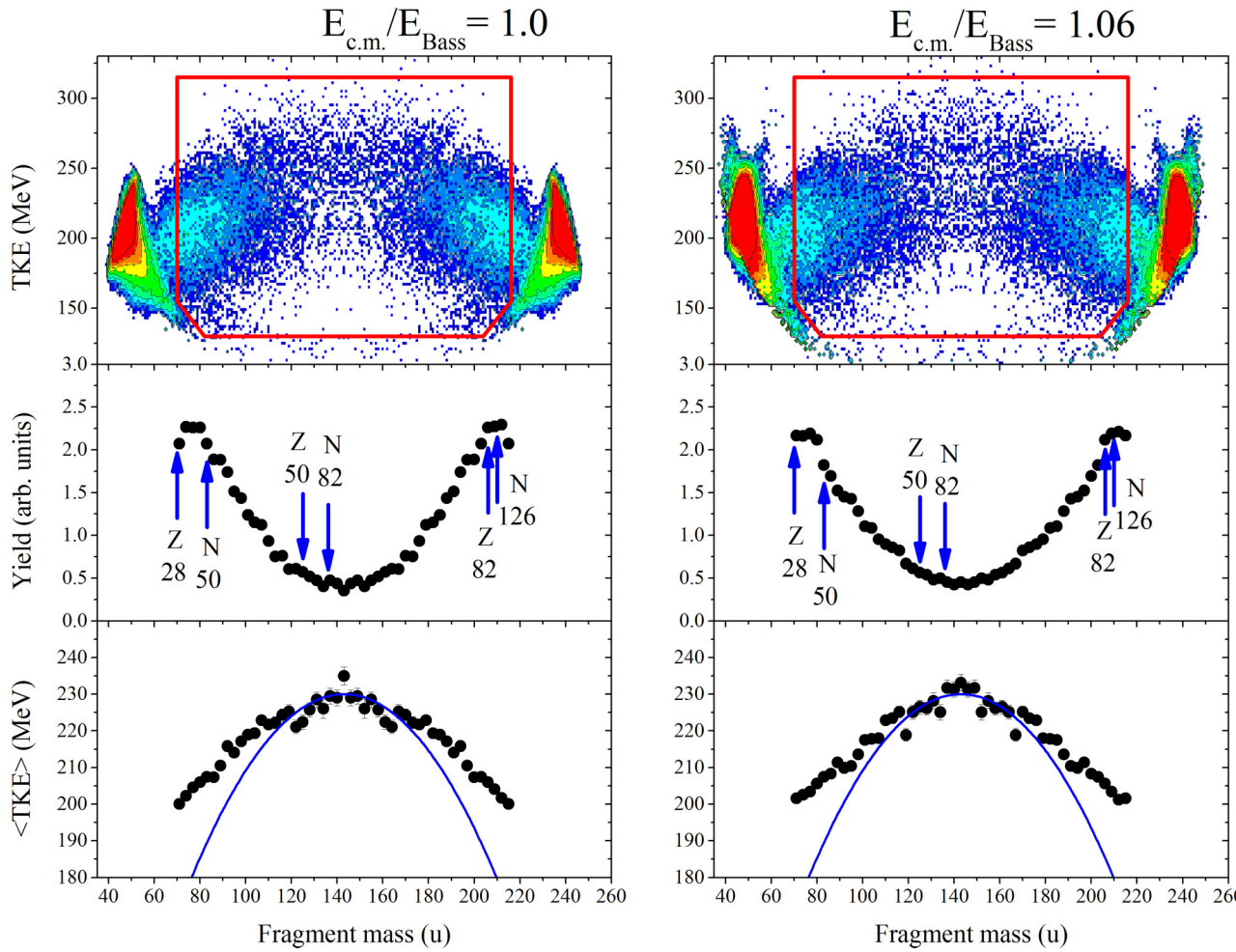

FIG. 1. The mass and energy distributions of binary fragments obtained in the ^{48}Ti + ^{238}U reaction at energies close to the Coulomb barrier [from top to bottom: the (TKE, *M*) matrices; the mass yields; the average TKEs as a function of mass for fissionlike events inside the outlined contours on the (TKE, *M*) matrices]. Solid lines in the average TKE distributions delineate the expectation from the liquid drop model. The arrows in the mass distributions indicate the positions of neutron and proton shells.

The middle and the bottom panels of Fig. 1 represent the mass and the average TKE distributions of fissionlike fragments inside the gates in (TKE, *M*) matrices for the ^{48}Ti + ^{238}U reaction. The mass spectra are normalized in such a way that the total area of each spectrum integrated over the mass range yields 200%. Solid curves in the ⟨TKE⟩ distributions are the descriptions of the liquid drop model component. The average TKE for symmetric fragments exhibits a parabolic dependence on mass, whereas for asymmetric QF fragments the deviations from the parabolic shape become significant. For fragments with masses of 200–210 u the experimental values of ⟨TKE⟩ are higher by 10–15 MeV than the liquid drop model prediction.

In Fig. 2 the mass distributions of fissionlike fragments for the ^{36}S, ^{48}Ca, ^{48}Ti, and ^{64}Ni + ^{238}U reactions at energies near and above the Coulomb barrier are shown. At first sight the distributions for the reaction of ^{48}Ti + ^{238}U are similar to those for the reactions with ^{48}Ca ions: The wide two-humped shape with the large QF component peaked around the mass of 208–210 u. In the case of the ^{36}S + ^{238}U reaction the asymmetric QF (QFasym) peaks around masses of 200 u and for ^{64}Ni + ^{238}U shifts to the heavier mass 215 u. As was already discussed in Refs. [24,25] the position of the asymmetric QF seems to be defined by the proton and neutron closed shells at $Z = 28, 82$ and $N = 50, 126$, and the deviation of the QF fragment masses from 208 u (double magic lead is expected to affect the formation of QF fragments strongly) is due to the influence of the shells $Z = 28$ and $N = 50$ in the light fragment. The driving potentials as a function of mass, shown in Fig. 2, have been calculated at contact configuration in the diabatic approximation within the proximity model with the aid of the Nuclear Reaction Vision Project (NRV) [32]. For the ^{36}S-ions-induced reaction the positions of the minima of the driving potential agree with the positions of the peaks in the experimental asymmetric QF mass distribution, whereas for the reactions with ^{48}Ti and ^{64}Ni the QFasym peak is shifted to the more asymmetric masses compared to the minimum of the driving potential.

One can see that in the case of the reactions with ^{36}S and ^{48}Ca ions the width of the asymmetric QF peak increases at higher interaction energy, whereas the mass distributions of fissionlike fragments formed in the reactions with ^{48}Ti and

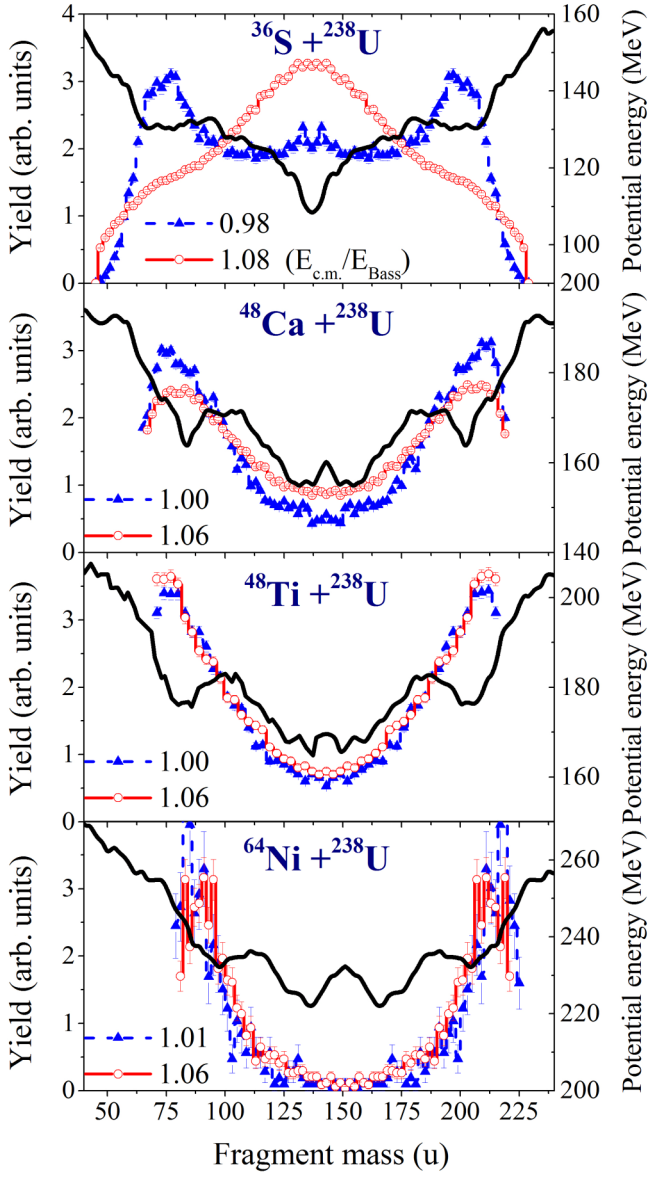

FIG. 2. Mass distributions of fissionlike fragments for the reactions ^{36}S, ^{48}Ca, ^{48}Ti, and ^{64}Ni + ^{238}U at energies near (the solid triangles) and above (the open circles) the Coulomb barrier together with potential energies of the systems at contact configuration (the thick lines). The incident energies ($E_{c.m.}/E_{Bass}$) are indicated at each plot.

^{64}Ni ions virtually do not change with the growing interaction energy. In the pioneering work of Shen *et al.* [10] it was found that the number of transferred nucleons for the QF process is connected with the reaction time. In the ^{48}Ca + ^{238}U reaction the experimental width of the QFasym mass distribution is about 27 u at the barrier energy and increases up to 38 u at 6% above the barrier, whereas in the reactions with ^{48}Ti and ^{64}Ni ions the widths of the QFasym peaks are nearly the same for both interaction energies and are about 25 and 12 u, respectively. Using the relation between the mass drift toward symmetry and the reaction time obtained by Shen *et al.* [10] and taking into account the strong influence of the closed shells on the formation of asymmetric QF fragments, the time scale for the QFasym process has been estimated in Ref. [33]. From the analysis of the QF mass distributions for the systems of ^{36}S, ^{48}Ca, and ^{64}Ni + ^{238}U it was found that the interaction time decreases exponentially with increasing Z_1Z_2 of the system [33,34]. The shift of the QFasym peak in the mass distribution to more asymmetric masses as well as the narrowing of its' width for the reactions with ^{48}Ti and ^{64}Ni ions as compared to the reactions with ^{36}S and ^{48}Ca ions may be explained by the shorter interaction time for the former reactions due to the larger Coulomb repulsion in the reaction entrance channel.

It should be noted that ^{238}U is a strongly deformed nucleus ($\beta_2 = 0.2863$ [35]). The relative orientation of deformed nuclei changes the Coulomb barrier due to the different distances between the centers of the colliding nuclei that affect the balance between repulsive and attractive forces. It was shown experimentally [18] that, if two interacting nuclei touch each other by their lateral surfaces (near-side collision), a high CN formation probability is expected, whereas in the elongated configuration when nuclei touch each other by their poles (near-tip collision), a QF probability is high (the so-called orientation effect). Recently the microscopic calculations based on the time-dependent Hartree-Fock theory performed for the reaction ^{40}Ca + ^{238}U [36] demonstrated that only tip collisions with ^{238}U produce QF fragments in the magic $Z = 82$ region, whereas collisions with the side are the only ones that may result in fusion. Also at side collisions the dinuclear system may undergo the QF process, but in this case the QF fragments are more symmetric, and the lead shell (at $Z = 82$ and $N = 126$) does not affect their formation.

As a first step to evaluate the CN-fission cross section the contribution of fragments with masses of $A_{CN}/2 \pm 20$ u can be considered. We may expect that the mass distributions of the CN-fission fragments can have symmetric Gaussian shapes with the standard deviation of about 20 u (see, for example, Ref. [25] for the case of Hs ($Z = 108$) nucleus) as predicted by the liquid drop model or asymmetric shape caused by the influence of the closed shells with $Z = 50$ and $N = 82$ as in the case of low-energy fission of actinides [34]. But in both cases the width of the CN-fission fragment mass distributions does not exceed 40 u, and the choice of the mass range of $A_{CN}/2 \pm 20$ u is reasonable.

The relative contributions of fragments with masses of $A_{CN}/2 \pm 20$ u into the capture cross section [fragments inside the rectangles in the (TKE, M) distributions in Fig. 1] for the reactions ^{238}U with ^{36}S, ^{48}Ca, ^{48}Ti, and ^{64}Ni ions are shown in Fig. 3. For the reactions under study the barrier for tip collisions is about 0.94 of the Coulomb barrier value and for the side collisions is about 1.03 [32]. At energies below the barrier for the side collisions the contribution of symmetric fragments increases with increasing collision energy, whereas above the barrier the yield of symmetric fragments increases with increasing collision energy for the reactions with ^{36}S and ^{48}Ca and does not change virtually for the reactions with ^{48}Ti and ^{64}Ni. In the recent paper of Nishio *et al.* [37] the mass distributions for the reaction ^{48}Ca + ^{238}U have been measured up to the energy of 20% above the barrier. At this energy ($E_{c.m.}/E_{Bass} = 1.27$) the mass

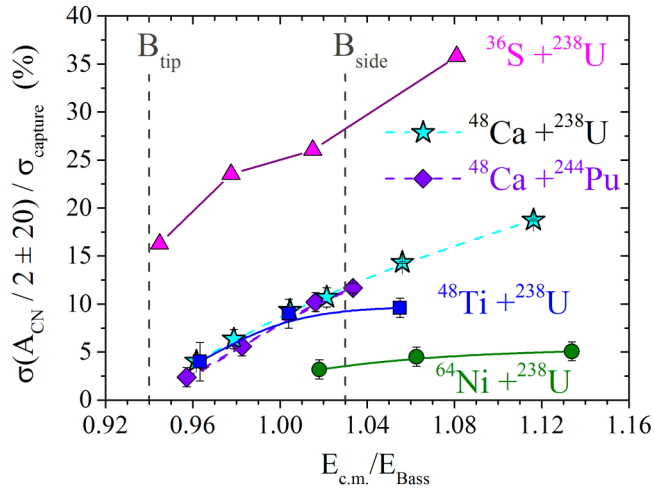

FIG. 3. Contributions of the symmetric fragments to the capture cross sections for the studied systems as a function of energy above the barrier.

distribution is mainly symmetric as in the case of the $^{36}S + ^{238}U$ reaction.

TKE distributions for the symmetric fragments with masses of $A_{CN}/2 \pm 20$ u for the reactions ^{36}S, ^{48}Ca, ^{48}Ti, and $^{64}Ni + ^{238}U$ are shown in Fig. 4. It is clearly seen that the TKE distributions change markedly showing nearly Gaussian shapes in the case of ^{36}S and ^{48}Ca ions and two-humped shapes for the reactions with ^{48}Ti and ^{64}Ni. One may speculate about the presence of other processes together with the CN fission in the symmetric mass region for the ^{36}S, ^{48}Ca, ^{48}Ti, and $^{64}Ni + ^{238}U$ reactions. We assume that the mass-symmetric fragments may be formed by three different modes: CN fission, symmetric QF (QFsym), and a tail of the asymmetric QF process. To evaluate the contribution of the CN-fission process in the symmetric mass region the TKE distributions are decomposed as a sum of three Gaussians. One of them is associated with the CN-fission process (filled region in Fig. 4).We fix the mean value and variance of this component to the values obtained from the systematics presented in Refs. [38,39], respectively. The low-energy component in Fig. 4 is attributed to QFasym whereas the high-energy one is connected with QFsym. As was shown in Ref. [25] in the case of the $^{58}Fe + ^{208}Pb$ reaction (where the asymmetric QF is a main process even in the symmetric mass region of fragments) the variance of TKE for QF does not depend on the mass of the QF fragments. At the fitting procedure we also fix the variance of the QFasym component equal to the variance of the TKE for the maximum yield of QFasym.

B. Fusion probabilities, capture, and CN-fission cross sections

P_{CN} is defined as the probability for CN formation from the configuration of two nuclei in contact. As was mentioned above, the cross section of the evaporation residues is approximately a few picobarns for these reactions. Thus we can deduce the fusion probability using the measured mass-energy distributions as the ratio between the number of events attributed to CN fission in the framework of the

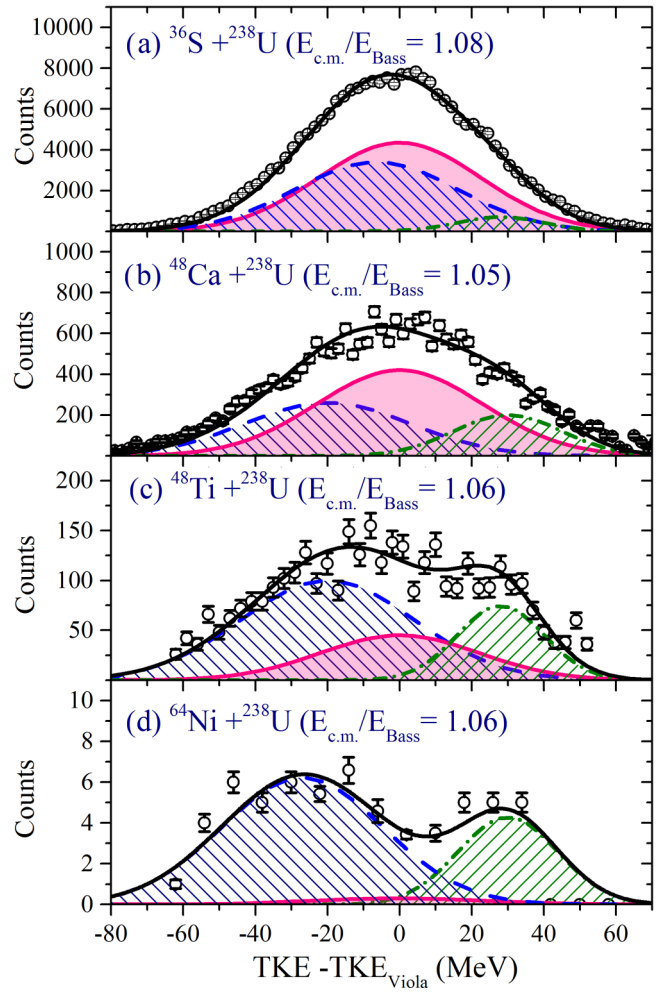

FIG. 4. TKE distributions of fragments with masses $A_{CN}/2 \pm 20$ u for the reactions ^{36}S, ^{48}Ca, ^{48}Ti, and $^{64}Ni + ^{238}U$ at energies above the Coulomb barrier. The filled region corresponds to the TKE distribution for CN fission. The dashed and dashed-dotted curves are associated with asymmetric and symmetric QF, respectively.

present analysis and all fissionlike fragments. In Fig. 5 the fusion probabilities in dependence on the energy above the Bass barrier for the studied reactions together with the data obtained for the reactions $^{48}Ca + ^{154}Sm$ [20], $^{26}Mg + ^{248}Cm$ [25], $^{48}Ca + ^{244}Pu$, and ^{248}Cm [24] are shown. Note that the target nuclei for all these reactions are strongly deformed.

The deduced values of P_{CN} in dependence on the interaction energy may be approximated by the simple formula proposed by Zagrebaev and Greiner [44] for fusion probability of cold fusion reactions,

$$P_{CN}(E_{c.m.}) = P_0/\{1 + \exp[\alpha(\beta - E_{c.m.}/E_{Bass})]\}, \quad (3)$$

where P_0, α, and β are empirical constants. P_0 is a fusion probability above the barrier, β is the effective barrier for CN formation, and α is responsible for the sub-barrier suppression of fusion probability. The differences between the estimated values of P_{CN} and the results of the fitting procedure are typically 2%–5% and do not exceed 10%.

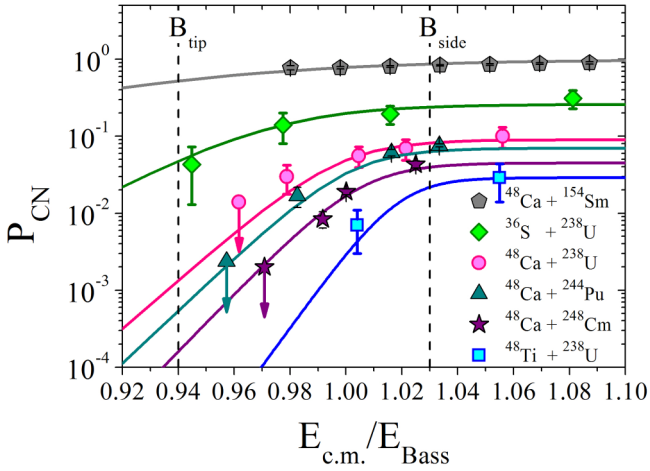

FIG. 5. The fusion probabilities obtained from the analysis of mass-energy distributions of fissionlike fragments for the reactions with strongly deformed target nuclei: ^{48}Ca + ^{154}Sm, ^{36}S + ^{238}U, ^{48}Ca + ^{238}U, ^{244}Pu, ^{248}Cm, and ^{48}Ti + ^{238}U.

The absolute differential cross sections for all fissionlike events observed in the reactions ^{36}S, ^{48}Ca, ^{48}Ti, and ^{64}Ni + ^{238}U were measured at an angle of $\theta_{\text{c.m.}} \approx 90^\circ$ at energies near the Coulomb barrier. Capture cross sections σ_{capture} for all fissionlike events were estimated assuming that the angular distribution is proportional to $\sin^{-1}\theta_{\text{c.m.}}$. This procedure seemed the most reasonable since detailed angular distributions are not available at present as well as any model (theory) for the angular distribution of fragments produced in the QF process.

The capture cross sections for the reactions ^{36}S, ^{48}Ca, and ^{64}Ni + ^{238}U have been reported in Refs. [23,24,40]. In the present paper the cross section for the reaction ^{48}Ti + ^{238}U has been measured at energies around the Coulomb barrier. In Fig. 6 the measured capture cross sections for all the studied reactions together with the capture cross sections from Refs. [8,37,41] are presented. The measured capture cross sections are described using the empirical model in the NRV code [32] (the solid lines in Fig. 6). The cross sections for the formation of symmetric fragments with masses of $A_{\text{CN}}/2 \pm 20$ u as well as the CN-fission cross section σ_{ff} deduced from the obtained fusion probabilities and capture cross sections are also presented in Fig. 6 (the dashed-dotted lines).

One can clearly see from Fig. 6 that the capture cross sections decrease at the transition from ^{36}S ions to ^{64}Ni. At energies above the barrier the capture cross sections for the reactions ^{36}S + ^{238}U and ^{48}Ca + ^{238}U are close to the geometrical cross sections, whereas for the ^{48}Ti + ^{238}U reaction it is about 60% of the geometrical cross section and about 15% in the case of the ^{64}Ni ions.

In Fig. 7 the measured capture cross sections as a function of effective fissility parameter x_{eff} are shown together with the data obtained for the reactions with ^{208}Pb [42] and ^{238}U [8] beams. For $x_{\text{eff}} \leqslant 0.75$ the capture cross sections virtually do not change. For x_{eff} larger than 0.75 the capture cross sections decrease exponentially with the increasing effective fissility parameter. Apparently for such systems, due to the large values of Z_1Z_2 that lead to the strong Coulomb repulsion between the interacting nuclei, the formation of the dinuclear system is inhibited. In this case the main reaction channel is a few-nucleon transfer process. For example, for the ^{64}Ni + ^{238}U reaction at an energy 13% above the barrier the capture cross section is 5.5 times lower than the total transfer cross section measured in Ref. [43]. However, as follows from the trend in σ_{capture} behavior, the orientation effect increases the probability to form the dinuclear system by several orders of magnitude for the reactions with large values of Z_1Z_2 that result in a slower decrease in the capture cross section in the reactions with U nuclei as compared to the reactions with Pb.

The CN-fission cross section decreases with increasing the effective fissility parameter of the system more crucially than the capture cross section. For instance, the CN-fission cross section decreases by several orders of magnitude at the transition from ^{48}Ca to ^{64}Ni ions, and at energies above the barrier it decreases from tens of millibarns to hundreds

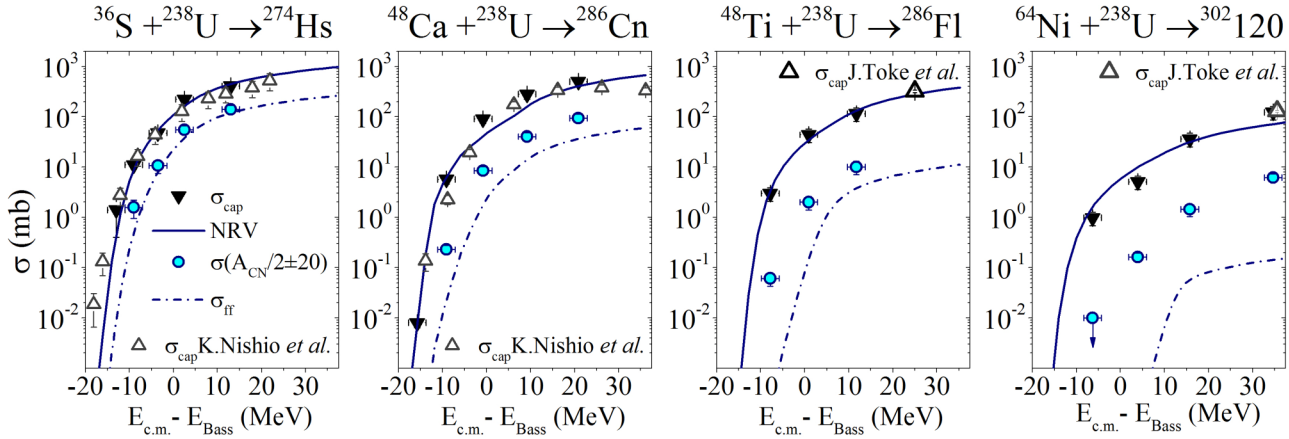

FIG. 6. The solid triangles are the cross sections for fissionlike fragments in the reactions ^{36}S, ^{48}Ca, ^{48}Ti, and ^{64}Ni + ^{238}U measured with the CORSET spectrometer, and the open triangles are the cross sections for fissionlike fragments from Refs. [8,37,41]. The solid lines are the empirical model calculations [32]. The circles are the cross sections for fragments with masses $A_{\text{CN}}/2 \pm 20$ u, and the dashed-dotted lines are the estimated CN-fission cross sections σ_{ff}.

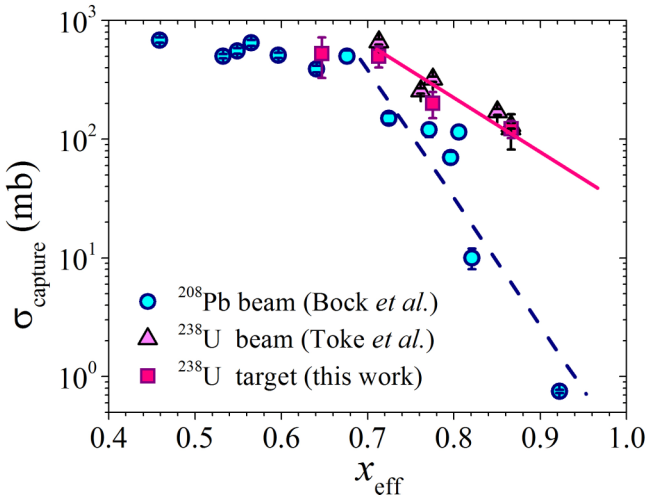

FIG. 7. The capture cross section as a function of the effective fissility parameter for the reactions with ^{208}Pb and ^{238}U nuclei at interaction energies of $E_{c.m.}/E_{Bass} = 1.1-1.2$. The lines are a guide for the eye.

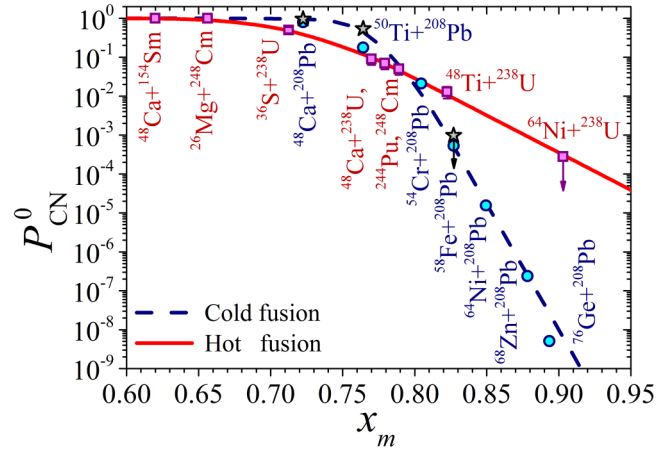

FIG. 8. Fusion probability in cold (spherical target nuclei) and hot fusion (strongly deformed target nuclei) reactions at energies above the Coulomb barrier in dependence on the mean fissility parameter of the reaction. The deduced fusion probabilities for the reactions with well-deformed target nuclei are shown by the squares, whereas for the reactions of Ca, Ti, and Fe ions with lead — by the stars. The circles are the fusion probabilities calculated for cold fusion reactions [44].

of microbarns. In the reaction $^{48}\mathrm{Ti} + {}^{238}\mathrm{U} \rightarrow {}^{286}\mathrm{Fl}^*$ the CN-fission cross section is about seven times lower as compared to the reaction $^{48}\mathrm{Ca} + {}^{244}\mathrm{Pu} \rightarrow {}^{292}\mathrm{Fl}^*$ [24].

C. Fusion probabilities at above barrier energies

As was already mentioned the fusion probability shows the general dependence on the effective fissility parameter connected with repulsive and attractive forces in the reaction entrance channel. Recently the analysis of a large bulk of data on mass-angle distributions of fissionlike fragments obtained in the reactions with heavy ions [30] has shown that the mean fissility parameter x_m defined as a linear combination between the effective fissility parameter x_{eff} and the true fissility parameter x_{CN}, reflecting the stability of CN with respect to fission,

$$x_m = 0.75x_{\mathrm{eff}} + 0.25x_{\mathrm{CN}} \tag{4}$$

is a better tool in the investigations of reaction mechanisms.

The dependence of fusion probability on the mean fissility parameter for the hot fusion reactions with strongly deformed targets, deduced from the present analysis of mass-energy distributions, is shown in Fig. 8. In this plot the data obtained for the reactions $^{48}\mathrm{Ca} + {}^{154}\mathrm{Sm}$ [20], $^{26}\mathrm{Mg} + {}^{248}\mathrm{Cm}$ [25], $^{48}\mathrm{Ca} + {}^{244}\mathrm{Pu}$, and $^{248}\mathrm{Cm}$ [24] are also presented. For all these reactions the target nuclei are well deformed. In the present paper the P_{CN} has been obtained as the ratio between the yield of CN fission and the experimental values of capture cross sections (see the previous subsection). However, the capture cross section is ambiguously defined both experimentally and theoretically. From an experimental point of view it is not so easy to separate elastic and quasielastic processes from capture events. Moreover, the angular distribution for QF is often not known. Therefore the angular distribution for all fissionlike events is assumed to be proportional to $\sin^{-1}\theta_{\mathrm{c.m.}}$ that increases the uncertainties of capture cross-sectional values. To avoid the additional errors connected with the disseminating of the capture cross section Zagrebaev and Greiner proposed using the contact cross section [44]. At above-barrier collision energies the contact cross section is close to the geometrical one. Thus the contact cross section can be approximately written as

$$\sigma_{\mathrm{cont}} = \pi R_B^2(1 - V^B/E_{\mathrm{c.m.}}). \tag{5}$$

To avoid the uncertainties connected with the definition of the capture cross section we renormalized the estimated value of P^0_{CN} to the contact cross section. In Fig. 8 we presented the values of fusion probabilities in dependence on the mean fissility parameter at above-barrier energy [P_0 values in Eq. (3)] when all orientations of interacting nuclei contribute into the formation of the dinuclear system. We compared our estimations with the fusion probabilities for the cold fusion reactions obtained by Zagrebaev and Greiner from the analysis of ER cross sections [44]. Along with them the fusion probabilities for the reactions ^{48}Ca ,^{50}Ti, and $^{58}\mathrm{Fe} + {}^{208}\mathrm{Pb}$ from Refs. [45,46,25] estimated using the same method based on the analysis of mass-energy distributions of fissionlike fragments are represented. One can see that within the error bars our data agree well with the estimations made by Zagrebaev and Greiner.

The fusion probabilities decrease exponentially with increasing the mean fissility parameter both for cold and for hot fusion reactions but with different rates. The solid and dashed lines in Fig. 8 are the descriptions of P^0_{CN} for hot and cold fusion reactions according to an equation proposed by Zagrebaev and Greiner [44],

$$P^0_{\mathrm{CN}} = \frac{1}{1 + \exp\left(\frac{x_m - \xi}{\tau}\right)}. \tag{6}$$

The parameters of Eq. (6) that give the best agreement with the estimated values of P^0_{CN} are as follows:

Reactions with Pb: $\tau = 0.0067 \pm 0.0007$; $\xi = 0.776 \pm 0.007$;

Reactions with actinide nuclei: $\tau = 0.0226 \pm 0.0006$; $\xi = 0.721 \pm 0.002$.

Such different behaviors of the $P_{\rm CN}^0$ dependence on the mean fissility parameter for the reactions with spherical and strongly deformed target nuclei may be explained by the orientation effect. In the case of spherical target nuclei the fusion probability is higher up to the values of mean fissility parameter $x_m \approx 0.8$, and for the larger values of x_m the fusion probability sharply decreases as compared to the reactions with strongly deformed target nuclei. As was already mentioned in the interactions of the deformed nuclei the orientation effect plays an important role in the evolution of the dinuclear system. Therefore, in the reactions with strongly deformed nuclei, QF starts to suppress CN formation at the lower values of x_m as compared to the reactions with spherical targets due to the contribution of near-tip collisions, whereas for $x_m > 0.8$ the near-side collisions give a gain in fusion probabilities even at large values of $Z_1 Z_2$.

These two cases of fusion probabilities for spherical target nuclei and strongly deformed ones give us the two limits. The fusion probabilities for deformed nuclei should lie somewhere between these curves since the orientation effect in these reactions is weaker than in the case of strongly deformed targets (actinide nuclei).

Notice that the fusion probabilities obtained from the analysis of mass-energy distributions of fissionlike fragments refer only to the upper limit. Another important feature of fissionlike fragments, which is to be taken into account in estimating the fusion probability, is their angular distribution [10]. However, as was mentioned above at the present time there is no model for angular distributions of QF fragments. As a result it is difficult to make meaningful estimations of the uncertainties in the deduced values of the fusion probabilities from the analysis of angular distributions. Nevertheless, with the help of Eq. (6) we can estimate the fusion probability decrease for production of the $Z = 120$ isotopes in the reactions with ^{50}Ti, ^{54}Cr, ^{58}Fe, and ^{64}Ni at above-barrier energies in comparison with the $^{48}\mathrm{Ca} + {}^{249}\mathrm{Cf} \rightarrow {}^{297}118^*$ reaction (the last reaction suitable for SHE synthesis using ^{48}Ca ions). Thus, it was found that the fusion probability for these reactions drops down about 10, 25, 90, and 110 times, respectively.

IV. SUMMARY

The mass and energy distributions of fissionlike fragments formed in the reactions $^{238}\mathrm{U} + {}^{36}\mathrm{S}$, $^{48}\mathrm{Ca}$, ^{48}Ti, and ^{64}Ni have been studied at energies around the Coulomb barrier. The measurements were performed using the double-arm time-of-flight spectrometer CORSET. The adequate mass and energy resolutions of the spectrometer allow exploring the structure of the mass and energy distributions.

At energies below the Coulomb barrier the main component of the distributions corresponds to the asymmetrical mass division typical for the asymmetric quasifission process. These quasifission fragments peak around the masses corresponding to closed neutron and proton shells. The position of the heavy quasifission fragments peak moves from 200 u for the $^{36}\mathrm{S} + {}^{238}\mathrm{U}$ reaction to 215 u for the $^{64}\mathrm{Ni} + {}^{238}\mathrm{U}$ reaction. Moreover, the width of asymmetric quasifission peaks in mass distributions increases with increasing interaction energy in the case of ^{36}S- and ^{48}Ca-ions-induced reactions, whereas in the case of ^{48}Ti and ^{64}Ni ions the widths virtually do not change that may point out that the interaction time for the latter reactions is shorter due to a larger Coulomb repulsion in the reaction entrance channel.

The contribution of symmetric fragments into all fissionlike events decreases at the transition from ^{36}S to ^{64}Ni ions. At energy above the Coulomb barrier the contribution of symmetric fragments into the capture process is about 40% for ^{36}S, 20% for ^{48}Ca, 8% for ^{48}Ti, and 5% for ^{64}Ni ions. It was found that significant parts of the symmetric fragments formed in the reactions $^{36}\mathrm{S}$ and $^{48}\mathrm{Ca} + {}^{238}\mathrm{U}$ have typical values of the mean total kinetic energies and their variances, which are inherent in CN fission. For the reactions with ^{48}Ti and ^{64}Ni the TKE distributions have two-humped shapes, and the kinetic energy expected for CN fission lies in the minimum between these two humps.

From the analysis of mass and TKE distributions the fusion probabilities have been estimated. At sub-barrier energies the obtained fusion probabilities are strongly suppressed. This suppression is the larger the heavier a system. The fusion probability at above-barrier energies decreases exponentially when the mean fissility parameter of the systems increases.

It was found that the fusion probability in the reactions with actinide target nuclei (strongly deformed ones) is several orders of magnitude higher than in the case of cold fusion reaction at the same value of mean fissility parameter for the systems with $x_m > 0.8$.

The capture cross section decreases with increasing the effective fissility parameter for the systems with $x_{\rm eff} > 0.75$ due to the large Coulomb repulsion in the entrance channel. The transfer process becomes dominant for the systems with $x_{\rm eff} > 0.8$. Besides, the capture cross sections decrease more slowly for the reactions with a U target nucleus compared with a Pb nucleus.

ACKNOWLEDGMENTS

We thank the staff of the U400 cyclotron for their careful work. This work was supported by the Russian Foundation for Basic Research (Grant No. 15-52-45098).

[1] A. Sobiczewski, F. A. Gareev, and B. N. Kalinkin, Phys. Lett. **22**, 500 (1966).

[2] S. Hofmann and G. Munzenberg, Rev. Mod. Phys. **72**, 733 (2000).

[3] S. Hofmann *et al.*, Eur. Phys. J. A **14**, 147 (2002).
[4] Y. T. Oganessian *et al.*, Phys. Rev. C **70**, 064609 (2004).
[5] Y. T. Oganessian *et al.*, Phys. Rev. C **74**, 044602 (2006).
[6] Y. T. Oganessian, J. Phys. G: Nucl. Part. Phys. **34**, R165 (2007).
[7] Y. T. Oganessian *et al.*, Phys. Rev. Lett. **104**, 142502 (2010).
[8] J. Toke *et al.*, Nucl. Phys. A **440**, 327 (1985).
[9] B. B. Back, H. G. Clerc, R. R. Betts, B. G. Glagola, and B. D. Wilkins, Phys. Rev. Lett. **46**, 1068 (1981).
[10] W. Q. Shen *et al.*, Phys. Rev. C **36**, 115 (1987).
[11] V. Zagrebaev and W. Greiner, J. Phys. G: Nucl. Part. Phys. **31**, 825 (2005).
[12] Y. Aritomo, K. Hagino, K. Nishio, and S. Chiba, Phys. Rev. C **85**, 044614 (2012).
[13] C. Simenel, Eur. Phys. J. A **48**, 152 (2012).
[14] G. G. Adamian, N. V. Antonenko, and W. Scheid, Phys. Rev. C **68**, 034601 (2003).
[15] R. S. Naik, W. Loveland, P. H. Sprunger, A. M. Vinodkumar, D. Peterson, C. L. Jiang, S. Zhu, X. Tang, E. F. Moore, and P. Chowdhury, Phys. Rev. C **76**, 054604 (2007).
[16] R. Yanez, W. Loveland, J. S. Barrett, L. Yao, B. B. Back, S. Zhu, and T. L. Khoo, Phys. Rev. C **88**, 014606 (2013).
[17] B. B. Back, R. R. Betts, J. E. Gindler, B. D. Wilkins, S. Saini, M. B. Tsang, C. K. Gelbke, W. G. Lynch, M. A. McMahan, and P. A. Baisden, Phys. Rev. C **32**, 195 (1985).
[18] D. J. Hinde, M. Dasgupta, J. R. Leigh, J. C. Mein, C. R. Morton, J. O. Newton, and H. Timmers, Phys. Rev. C **53**, 1290 (1996); J. C. Mein, D. J. Hinde, M. Dasgupta, J. R. Leigh, J. O. Newton, and H. Timmers, *ibid.* **55**, R995 (1997).
[19] D. J. Hinde, A. C. Berriman, R. D. Butt, M. Dasgupta, C. R. Morton, A. Mukherjee, and J. O. Newton, Eur. Phys. J. A **13**, 149 (2002).
[20] G. N. Knyazheva *et al.*, Phys. Rev. C **75**, 064602 (2007).
[21] R. G. Thomas, D. J. Hinde, D. Duniec, F. Zenke, M. Dasgupta, M. L. Brown, M. Evers, L. R. Gasques, M. D. Rodriguez, and A. Diaz-Torres, Phys. Rev. C **77**, 034610 (2008).
[22] T. K. Ghosh *et al.*, Phys. Rev. C **79**, 054607 (2009).
[23] E. M. Kozulin *et al.*, Phys. Lett. B **686**, 227 (2010).
[24] E. M. Kozulin *et al.*, Phys. Rev. C **90**, 054608 (2014).
[25] I. M. Itkis *et al.*, Phys. Rev. C **83**, 064613 (2011).
[26] B. B. Back, P. B. Fernandez, B. G. Glagola, D. Henderson, S. Kaufman, J. G. Keller, S. J. Sanders, F. Videbæk, T. F. Wang, and B. D. Wilkins, Phys. Rev. C **53**, 1734 (1996).
[27] D. J. Hinde, R. G. Thomas, R. du Rietz, A. Diaz-Torres, M. Dasgupta, M. L. Brown, M. Evers, L. R. Gasques, R. Rafiei, and M. D. Rodriguez, Phys. Rev. Lett. **100**, 202701 (2008).
[28] D. J. Hinde, R. du Rietz, M. Dasgupta, R. G. Thomas, and L. R. Gasques, Phys. Rev. Lett. **101**, 092701 (2008).
[29] R. du Rietz, D. J. Hinde, M. Dasgupta, R. G. Thomas, L. R. Gasques, M. Evers, N. Lobanov, and A. Wakhle, Phys. Rev. Lett. **106**, 052701 (2011).
[30] R. du Rietz, E. Williams, D. J. Hinde, M. Dasgupta, M. Evers, C. J. Lin, D. H. Luong, C. Simenel, and A. Wakhle, Phys. Rev. C **88**, 054618 (2013).
[31] E. M. Kozulin *et al.*, Instrum. Exp. Tech. **51**, 44 (2008).
[32] http://nrv.jinr.ru/nrv
[33] G. N. Knyazheva, I. M. Itkis, and E. M. Kozulin, J. Phys.: Conf. Ser. **515**, 012009 (2014).
[34] M. G. Itkis, E. Vardaci, I. M. Itkis, G. N. Knyazheva, and E. M. Kozulin, Nucl. Phys. A **944**, 204 (2015).
[35] S. Raman, C. W. Nestor, Jr., and P. Tikkanen, At. Data Nucl. Data Tables **78**, 1 (2001).
[36] A. Wakhle, C. Simenel, D. J. Hinde, M. Dasgupta, M. Evers, D. H. Luong, R. du Rietz, and E. Williams, Phys. Rev. Lett. **113**, 182502 (2014).
[37] K. Nishio, S. Mitsuoka, I. Nishinaka, H. Makii, Y. Wakabayashi, H. Ikezoe, K. Hirose, T. Ohtsuki, Y. Aritomo, and S. Hofmann, Phys. Rev. C **86**, 034608 (2012).
[38] V. E. Viola, K. Kwiatkowski, and M. Walker, Phys. Rev. C **31**, 1550 (1985).
[39] M. G. Itkis and A. Ya. Rusanov, Phys. Part. Nucl. **29**, 160 (1998).
[40] M. G. Itkis, I. M. Itkis, G. N. Knyazheva, and E. M. Kozulin, Nucl. Phys. A **834**, 374 (2010).
[41] K. Nishio, H. Ikezoe, S. Mitsuoka, I. Nishinaka, Y. Nagame, Y. Watanabe, T. Ohsuki, K. Hirose, and S. Hofman, Phys. Rev. C **77**, 064607 (2008).
[42] R. Bock *et al.*, Nucl. Phys. A **388**, 334 (1982).
[43] L. Corradi, A. M. Stefanini, C. J. Lin, S. Beghini, G. Montagnoli, F. Scarlassara, G. Pollarolo, and A. Winther, Phys. Rev. C **59**, 261 (1999).
[44] V. I. Zagrebaev and W. Greiner, Nucl. Phys. A **944**, 257 (2015).
[45] E. V. Prokhorova *et al.*, Nucl. Phys. A **802**, 45 (2008).
[46] M. G. Itkis *et al.*, Nucl. Phys. A **787**, 150 (2007).